Supplementary Text: Speed of invasion of an expanding population by a horizontally-transmitted trait

Juan Venegas-Ortiz, Rosalind J. Allen and Martin R. Evans

I. STABILITY ANALYSIS OF FIXED POINTS

Here we discuss the stability of the fixed point of our key equations (Eqs 3 in the main text). This equation set can be rewritten as

$$\begin{aligned}\frac{\partial N_{\rm A}}{\partial t} &= D\frac{\partial^2 N_{\rm A}}{\partial x^2} + \alpha N_{\rm A}(K - N_{\rm T}) - \beta N_{\rm A} + \gamma N_{\rm A} N_{\rm B} \\ \frac{\partial N_{\rm T}}{\partial t} &= D\frac{\partial^2 N_{\rm T}}{\partial x^2} + \alpha N_{\rm T}(K - N_{\rm T})\,. \end{aligned} \tag{1}$$

where the first equation is identical to the equation for $N_{\rm A}$ in the main text, and the second equation has been obtained by summing the equations for $N_{\rm A}$ and $N_{\rm B}$. The fixed points of Eqs. (1) satisfy

$$\begin{aligned}\alpha N^*_{\rm A}(K - N^*_{\rm T}) - \beta N^*_{\rm A} + \gamma N^*_{\rm A} N^*_{\rm B} &= 0 \\ \alpha N^*_{\rm T}(K - N^*_{\rm T}) &= 0\,. \end{aligned} \tag{2}$$

The three relevant solutions of these equations are
(i) $(N^*_T, N^*_A) = (0, 0)$: this is the trivial case where both populations are zero.
(ii) $(N^*_T, N^*_A) = (K, 0)$: this solution describes a domain full with individuals that do not carry the trait; no trait-carrying individuals are present.
(iii) $(N^*_T, N^*_A) = (K, K - \beta/\gamma)$: this solution is the most interesting one for our purposes. It describes a domain which contains coexisting subpopulations of trait-carrying and non-trait carrying individuals. This solution is only valid if $\gamma \geq \beta/K$ (such that $N^*_A > 0$) - i.e. if the rate of horizontal transmission is high enough that the trait can be sustained in the population.
We note that mathematically there is also another solution $(N^*_T, N^*_A) = (0, (K\alpha - \beta)/\gamma)$; however this is not physically relevant, since it implies that $N^*_A = -N^*_B$ - i.e. one of the subpopulations has a negative density.

We now perform a standard linear stability analysis [1], in which we consider small perturbations about the homogeneous fixed point solutions: i.e. $(N_T, N_A) = (N^*_T + \epsilon, N^*_A + \eta)$. The fate of these perturbations can be described by:

$$\frac{\partial}{\partial t}\begin{pmatrix}\epsilon\\ \eta\end{pmatrix} = M\begin{pmatrix}\epsilon\\ \eta\end{pmatrix} \tag{3}$$

where M is the Jacobian matrix, given by

$$M = \begin{pmatrix}\alpha(K - 2N^*_{\rm T}) & 0\\ -(\alpha - \gamma)N^*_{\rm A} & \alpha(K - N^*_{\rm T}) - \beta + \gamma(N^*_{\rm T} - 2N^*_{\rm A})\end{pmatrix}. \tag{4}$$

This matrix has two eigenvalues, given by $\lambda_1 = \alpha(K - 2N^*_{\rm T})$ and $\lambda_2 = \alpha(K - N^*_{\rm T}) - \beta + \gamma(N^*_{\rm T} - 2N^*_{\rm A})$. Following the standard approach in linear stability analysis [1], we can deduce the stability of the fixed points from the sign of the eigenvalues, evaluated at the fixed points. Specifically, we find that

- The fixed point $(N^*_T, N^*_A) = (0, 0)$ has eigenvalues $\lambda_1 = \alpha K$ and $\lambda_2 = \alpha K - \beta$. These are both positive under the conditions considered in this work, i.e. $\beta < \gamma K$ and $\gamma < \alpha$. Thus, this fixed point is unstable.
- The fixed point $(N^*_T, N^*_A) = (K, 0)$ has eigenvalues $\lambda_1 = -\alpha K$ and $\lambda_2 = \gamma K - \beta$. The first eigenvalue is always negative (for reasonable parameters α and K). The second eigenvalue λ_2 is positive for the parameter values considered in this work, i.e. for $\beta < \gamma K$. This implies that this fixed point is a saddle point.
- The fixed point $(N^*_T, N^*_A) = (K, K - \beta/\gamma)$ has eigenvalues $\lambda_1 = -\alpha K$ and $\lambda_2 = \beta - \gamma K$. Under the conditions considered here, i.e. $\beta < \gamma K$, both these eigenvalues are negative. Thus this fixed point is stable.

The coupled travelling waves which we observe in our numerical simulations correspond to a homogeneous spatial domain containing the solution $(0, 0)$ being invaded by the solution $(K, 0)$ (i.e. a population wave which does not carry the trait), and, in turn, the domain containing the solution $(K, 0)$ being invaded by the solution $(K, K - \beta/\gamma)$ (i.e. the trait wave).

II. FISHER-KPP WAVE THEORY

We now discuss in more detail the principles of F-KPP wave theory, which form the starting point of our analysis in the main text. We consider the standard F-KPP equation

$$\frac{\partial u}{\partial t} = D\frac{\partial^2 u}{\partial x^2} + \alpha u(K-u) \tag{5}$$

Eq. (5) has traveling wave solutions of the form $u(x,t) = U(x-vt)$. This implies that at large times the population asymptotically expands in a wave of constant shape which moves at a constant speed v, as illustrated in Fig. 1(a) of the main text. The main part of the wave (the "front") is preceded by a low-density "tip" which extends ahead of the front. The dynamics in this tip region is crucial in controlling the wave speed v.

The selection principle that controls the wave speed states that if the initial profile decays faster than $u(x,0) \sim \mathrm{e}^{-\lambda^* x}$, where $\lambda^* = v^*/2D$, then the wave travels at the well-known Fisher speed $v = v^* = 2\sqrt{\alpha D K}$; whereas if the initial profile decays less steeply, say as $\mathrm{e}^{-\lambda x}$ where $\lambda < \lambda^*$, the wave advances at a faster, initial condition-dependent speed $v = D\lambda + \alpha K/\lambda$.

The origin of this speed selection principle can be understood as follows [2]. We consider the dynamics at the tip of the profile, where u is small and Eq. (5) can be linearized as

$$\frac{\partial u}{\partial t} = D\frac{\partial^2 u}{\partial x^2} + \alpha K u \; . \tag{6}$$

This linearized equation can be solved exactly and for the initial condition of an exponential profile $u(x,0) = \mathrm{e}^{-\lambda x}$ for $x \geq 0$, the solution reads

$$u(x,t) = (1/2)e^{-\lambda(x-v(\lambda)t)}\left[1 + \mathrm{erf}\Big((x-2D\lambda t)/(2\sqrt{Dt})\Big)\right] \tag{7}$$

where

$$v(\lambda) = D\lambda + \frac{\alpha K}{\lambda} \; . \tag{8}$$

Careful inspection of this solution reveals that different parts of the wave profile actually move at different speeds. At the very tip of the profile, where $x \gg 2D\lambda t$, we can use $\mathrm{erf}(z) \simeq 1$ for $z \gg 1$ and the solution reduces to $u(x,t) \simeq e^{-\lambda(x-v(\lambda)t)}$; thus the tip advances with speed $v(\lambda)$ that is entirely controlled by the initial condition. However, further back in the wave profile, where $x \ll 2D\lambda t$ (but u is still small) expanding the error function as $\mathrm{erf}(-z) \simeq -1 + \frac{\mathrm{e}^{-z^2}}{z\sqrt{\pi}}$ for $z \gg 1$ yields $u \simeq e^{-\lambda^*(x-v^*t)-(x-v^*t)^2/(4Dt)}$, where $v^* = 2(D\alpha K)^{1/2}$. The crossover point between these two regimes occurs at the point in the profile where $x = 2D\lambda t$. If $\lambda > \lambda^* = v^*/2D$, then the crossover point advances faster than the tip, and the main part of the wave (the "front") will advance at speed v^*. However, if $\lambda < \lambda^*$, the crossover point falls behind the tip, and, for long times, the speed of the front will be controlled by the tip; thus the wave moves at speed $v(\lambda)$ determined by the initial condition.

III. NUMERICAL SIMULATIONS

Here, we discuss in detail the method used to propagate the population densities $N_{\mathrm{A}}(x,t)$ and $N_{\mathrm{B}}(x,t)$ in time and space in our numerical simulations. Our equation set

$$\begin{aligned}
\frac{\partial N_{\mathrm{B}}}{\partial t} &= D\frac{\partial^2 N_{\mathrm{B}}}{\partial x^2} + \alpha N_{\mathrm{B}}(K - N_{\mathrm{T}}) + \beta N_{\mathrm{A}} - \gamma N_{\mathrm{A}} N_{\mathrm{B}} \\
\frac{\partial N_{\mathrm{A}}}{\partial t} &= D\frac{\partial^2 N_{\mathrm{A}}}{\partial x^2} + \alpha N_{\mathrm{A}}(K - N_{\mathrm{T}}) - \beta N_{\mathrm{A}} + \gamma N_{\mathrm{A}} N_{\mathrm{B}} \; ,
\end{aligned} \tag{9}$$

(Eqs 3 in the main text) are discretized in time and space and propagated on a one-dimensional spatial lattice, with grid spacing $\Delta x = 0.1$ and time step $\Delta t = 0.001$. We use an operator splitting method [3], in which the diffusion term in the equations is propagated using an implicit Crank-Nicolson scheme [3], while the growth and horizontal transfer

terms are propagated using explicit forward Euler integration. This scheme is described in more detail below. It provides enhanced stability over fully explicit Euler integration [3]; however we have verified that essentially identical results are obtained using a fully explicit simulation scheme.

As our initial condition, we set the population densities at the edge of the domain ($x = 0$) to the steady-state solutions $N_{\rm A} = K - \beta/\gamma$ and $N_{\rm B} = \beta/\gamma$. The population densities in the rest of the spatial lattice are usually set to zero (to simulate a trait wave invading an expanding population), but may take other forms (e.g. for a trait wave invading an established population we set $N_{\rm B} = K$ in the rest of the domain).

Each update step in our algorithm consists of the following procedure:

1. Update the subpopulations using the diffusion terms only, via an implicit Crank-Nicolson scheme [3]. This means that we update the subpopulations $N_{\rm A}^{(j)}$ and $N_{\rm B}^{(j)}$ (where j denotes the j-th position on the spatial lattice site), according to

$$\frac{N_{\rm A}^{(j,{\rm new})} - N_{\rm A}^{(j,{\rm old})}}{\Delta t} = \frac{D}{2}\left[\frac{\left(N_{\rm A}^{(j+1,{\rm new})} - 2N_{\rm A}^{(j,{\rm new})} + N_{\rm A}^{(j-1,{\rm new})}\right) + \left(N_{\rm A}^{(j+1,{\rm old})} - 2N_{\rm A}^{(j,{\rm old})} + N_{\rm A}^{(j-1,{\rm old})}\right)}{(\Delta x)^2}\right] \tag{10}$$

   (with an equivalent update for $N_{\rm B}$). This set of coupled linear equations is solved for $N_{\rm A}^{(j,{\rm new})}$ (and $N_{\rm B}^{(j,{\rm new})}$) using a tridiagonal matrix method (*Tridag* from [3]).

2. Set $N_{\rm A}^{(j,{\rm new})} \to N_{\rm A}^{(j,{\rm old})}$ and $N_{\rm B}^{(j,{\rm new})} \to N_{\rm B}^{(j,{\rm old})}$.

3. Update the subpopulations using the terms for growth, horizontal transmission and loss of the trait only, using explicit forward Euler integration. This means that we update according to

$$\frac{N_{\rm A}^{(j,{\rm new})} - N_{\rm A}^{(j,{\rm old})}}{\Delta t} = \alpha N_{\rm A}^{(j,{\rm old})}\left[K - \left(N_{\rm A}^{(j,{\rm old})} + N_{\rm B}^{(j,{\rm old})}\right)\right] - \beta N_{\rm B}^{(j,{\rm old})} + \gamma N_{\rm A}^{(j,{\rm old})} N_{\rm B}^{(j,{\rm old})} \tag{11}$$

$$\frac{N_{\rm B}^{(j,{\rm new})} - N_{\rm B}^{(j,{\rm old})}}{\Delta t} = \alpha N_{\rm B}^{(j,{\rm old})}\left[K - \left(N_{\rm A}^{(j,{\rm old})} + N_{\rm B}^{(j,{\rm old})}\right)\right] + \beta N_{\rm B}^{(j,{\rm old})} - \gamma N_{\rm A}^{(j,{\rm old})} N_{\rm B}^{(j,{\rm old})} \tag{12}$$

4. Set $N_{\rm A}^{(j,{\rm new})} \to N_{\rm A}^{(j,{\rm old})}$ and $N_{\rm B}^{(j,{\rm new})} \to N_{\rm B}^{(j,{\rm old})}$, and update time $t \to t + \Delta t$.

This update step is repeated throughout the course of the simulation.

To measure the front speed of the total population and trait waves, we track in time the spatial location where the population density is half-maximal: i.e. $N_{\rm B}(x) = K/2$ or $N_{\rm A}(x) = (K - \beta/\gamma)/2$. This position is determined by linear interpolation between points on the discrete lattice. The front position is plotted as a function of time, (as in Fig. 2 of the main text), and the gradient of this plot (computed by least squares fitting) is used as a measure of the front speed. The front speed is only measured once the dependence of the front position on time has become (approximately) linear.

To track the speed of the very tip of the trait wave, we follow a similar procedure, but this time following the position at which $N_{\rm A}(x) = 10^{-323}$, which is the limit of resolution of our double precision simulations.

IV. EXTENSION TO THE NON-NEUTRAL CASE

To investigate whether the speed selection mechanism described in this work still holds for the non-neutral case, we carried out numerical simulations for the following extension of the basic model:

$$\begin{aligned}
\frac{\partial N_{\rm B}}{\partial t} &= D\frac{\partial^2 N_{\rm B}}{\partial x^2} + \alpha_{\rm A} N_{\rm B}(K - N_{\rm T}) + \beta N_{\rm A} - \gamma N_{\rm A} N_{\rm B} \\
\frac{\partial N_{\rm A}}{\partial t} &= D\frac{\partial^2 N_{\rm A}}{\partial x^2} + \alpha_{\rm B} N_{\rm A}(K - N_{\rm T}) - \beta N_{\rm A} + \gamma N_{\rm A} N_{\rm B}
\end{aligned} \tag{13}$$

In Eqs (13), if $\alpha_{\rm A} > \alpha_{\rm B}$, the horizontally transmitted trait confers a selective advantage (i.e. an increased growth rate), compared to individuals that do not carry the trait. In contrast, if $\alpha_{\rm A} < \alpha_{\rm B}$, there is a selective disadvantage

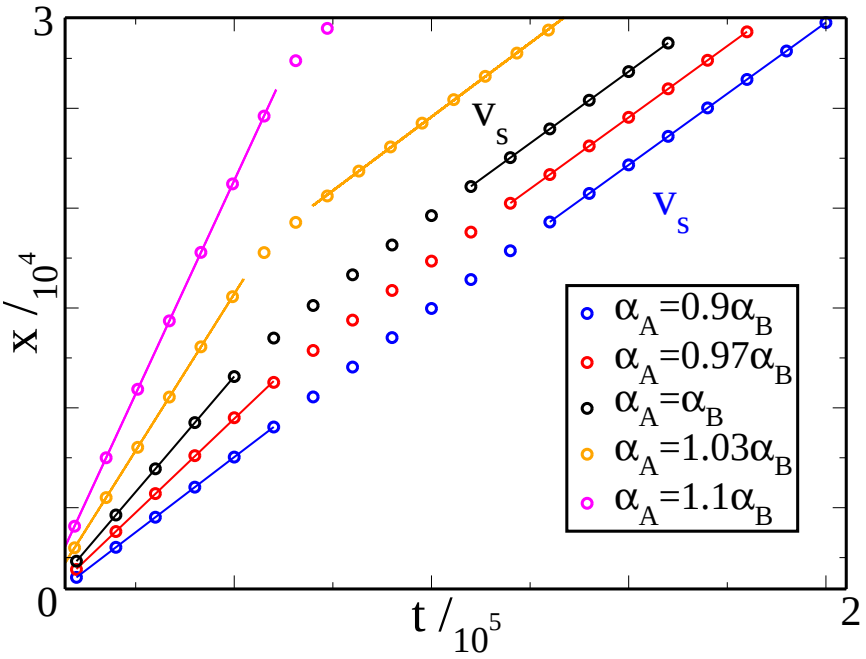

Figure S 1: Numerical results for the propagation of the front of the trait wave into an expanding population, for different scenarios for the relative growth rates of trait-carrying and non-trait carrying individuals. The case $\alpha_A = \alpha_B$ (black symbols) corresponds to the same parameter set as in the main text ($K = 1, D = 1, \alpha_A = \alpha_B = 1, \beta = 0.08$ and $\gamma = 0.1$). The colored symbols show results for simulations where the two subpopulations have different growth rates. All simulations are initiated with the spatial domain empty apart from at the left hand side (as in the bottom panels of Fig. 2 in the main text).

for trait-carrying individuals.

Fig.S 1 shows the position of the front of the trait wave as a function of time, for simulations in which the trait invades an expanding population: i.e. the domain is initially empty and the population spreads as two coupled waves (the "outer", total population wave and the "inner" trait wave). The neutral case ($\alpha_A = \alpha_B$) is shown in black; this shows a transition from a faster wave speed v_c (given by Eq. (7) in the main text), corresponding to invasion of an expanding population, to the slower speed $v_s = 2\sqrt{D(\gamma K - \beta)}$, which corresponds to invasion of an established population. These results are the same as those in the main text, Fig. 2 (bottom left panel). The colored symbols show results for the non-neutral case. The red and blue symbols are for the case where $\alpha_A < \alpha_B$ i.e. the trait is detrimental to fitness. This data shows that for a small fitness disadvantage (here 3%), the same behaviour holds, but the speedup factor for invasion of the expanding population is smaller (i.e. the initial speed is lower) than in the neutral case. For a larger fitness disadvantage (here 10%) the initial speedup is barely noticeable. The orange and magenta symbols show results for the case where $\alpha_A > \alpha_B$ - i.e. the trait is advantageous. Here again, we see a speedup in the speed of invasion of the trait as it invades an expanding population; in this case the "speedup factor" is actually greater than in the neutral case and increases with the fitness advantage. Here also we eventually see a reversion to the universal speed v_s once the total population and trait waves become decoupled.

[1] S. H. Strogatz *Nonlinear dynamics and chaos* (Westview Press, 1994).
[2] W. van Saarloos (2003) Front propagation into unstable states. *Phys Rep* 386:29-222.
[3] W. H. Press, S. A. Teukolsky, W. T. Vetterling and B. P. Flannery *Numerical Recipes in Fortran 77. The art of Scientific Computing. Second Edition.* (Cambridge University Press, 1992).